Research Article

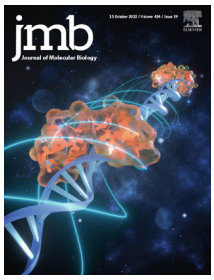

Dityrosine Cross-links are Present in Alzheimer's Disease-derived Tau Oligomers and Paired Helical Filaments (PHF) which Promotes the Stability of the PHF-core Tau (297–391) *In Vitro*

Mahmoud B. Maina [1,2], Youssra K. Al-Hilaly [1,3], Sebastian Oakley [1], Gunasekhar Burra [1,4], Tahmida Khanom [1], Luca Biasetti [1], Kurtis Mengham [1], Karen Marshall [1], Charles R. Harrington [5,6], Claude M. Wischik [5,6] and Louise C. Serpell [1]*

*1 - **Sussex Neuroscience,** School of Life Sciences, University of Sussex UK*
*2 - **Biomedical Science Research and Training Centre,** Yobe State University, Nigeria*
*3 - **Chemistry Department,** College of Sciences, Mustansiriyah University, Baghdad, Iraq*
*4 - **Analytical Development Biologics,** Biopharmaceutical Development, Syngene International Limited, Biocon Park, Bommasandra Jigani Link Road, Bangalore 560009, India*
*5 - **Institute of Medical Sciences,** University of Aberdeen, UK*
*6 - **TauRx Therapeutics Ltd,** Aberdeen, UK*

***Correspondence to Louise C. Serpell:** L.C.Serpell@sussex.ac.uk (L.C. Serpell) @mahmoudbukar (M.B. Maina), @serpelllab, @serpell1 (L.C. Serpell)*
https://doi.org/10.1016/j.jmb.2022.167785
Edited by Daniel Otzen

Abstract

A characteristic hallmark of Alzheimer's Disease (AD) is the pathological aggregation and deposition of tau into paired helical filaments (PHF) in neurofibrillary tangles (NFTs). Oxidative stress is an early event during AD pathogenesis and is associated with tau-mediated AD pathology. Oxidative environments can result in the formation of covalent dityrosine crosslinks that can increase protein stability and insolubility. Dityrosine cross-linking has been shown in Aβ plaques in AD and α-synuclein aggregates in Lewy bodies in ex vivo tissue sections, and this modification may increase the insolubility of these aggregates and their resistance to degradation. Using the PHF-core tau fragment (residues 297 – 391) as a model, we have previously demonstrated that dityrosine formation traps tau assemblies to reduce further elongation. However, it is unknown whether dityrosine crosslinks are found in tau deposits *in vivo* in AD and its relevance to disease mechanism is unclear. Here, using transmission electron microscope (TEM) double immunogold-labelling, we reveal that neurofibrillary NFTs in AD are heavily decorated with dityrosine crosslinks alongside tau. Single immunogold-labelling TEM and fluorescence spectroscopy revealed the presence of dityrosine on AD brain-derived tau oligomers and fibrils. Using the tau (297–391) PHF-core fragment as a model, we further showed that prefibrillar tau species are more amenable to dityrosine crosslinking than tau fibrils. Dityrosine formation results in heat and SDS stability of oxidised prefibrillar and fibrillar tau assemblies. This finding has implications for understanding the mechanism governing the insolubility and toxicity of tau assemblies *in vivo*.

Introduction

Tau protein was first described as a cytoplasmic protein that plays a role in microtubule dynamics.[1–2] However, recent evidence suggests that it plays multiple functions, including DNA protection, heterochromatin stability and nucleolar transcription.[3–6] Interest in tau intensified following the discovery that it is the main component of the intracellular neurofibrillary tangles (NFTs), comprised of straight (SFs) and paired-helical filaments (PHFs), which forms one of the hallmarks of Alzheimer's disease (AD), alongside extracellular deposits of amyloid-beta (Aβ).[7–10] Under native conditions, tau is soluble and intrinsically disordered. However, post-translational modifications, truncation, mutations or cellular stress conditions influence its structure and propensity to aggregate.[11–12] In disease, SFs and PHFs are formed from the assembly of tau monomers to dimers, then oligomers and eventually fibrils, which deposit as NFTs, although the specific disease causing species has not been identified. For example, while phosphorylation,[13] truncation,[8,14] or cysteine oxidation have been shown to promote tau aggregation,[15] other modifications, such as nitration of tyrosine residues inhibit tau nucleation and/or elongation[16–17] and glycation stabilises filaments and increases insolubility of NFTs.[18–19]

The longest central nervous system isoform of human tau has five tyrosines, at positions 18, 29, 197, 310, and 394. In addition to nitration, these residues are targets of other post-translational modifications, including phosphorylation and dityrosine cross-linking (Figure S1(a)). All of these alterations could result in the accumulation of oligomers.[17,20–23] To understand the contribution of dityrosine formation on tau, we have recently reported a new tau model for *in vitro* studies of aggregation of a 95 amino acid tau fragment comprised of residues Ile-297–Glu-391 of the full-length tau, also referred to as dGAE.[24] The dGAE fragment was previously isolated from the proteolytically stable PHF core[8] and overlaps with the core of AD PHFs revealed by cryo-electron microscopy[25] (Figure S1(b)). dGAE assembles into filaments without the need for additives such as heparin or arachidonic acid[24,26] and is able to form an identical structure to ex-vivo filaments extracted from AD and Chronic Traumatic Encephalopathy (CTE).[27]

Using metal-catalysed oxidation (MCO), we previously showed that oxidation of dGAE (which contains tyrosine 310) results in rapid formation of dityrosine crosslinked tau oligomers, which lack the ability to elongate into fibrils, suggesting that the dityrosine bond formation results in the stabilisation of the oligomers,[23] similar to Aβ oligomers.[28] Consistent with this, $ONOO^-$-treated full-length tau filaments in an arachidonic acid model of tau aggregation was previously shown to increase filament stability[29] similar to stability and insolubility of brain-derived PHFs.[30–32]

Given the high stability and irreversibility of the dityrosine covalent bonding,[33] crosslinked proteins can be detected in various *in vitro* and *in vivo* settings. Aβ and α-synuclein have both been shown to form dityrosine cross-links in *vitro,* and dityrosine cross-linked Aβ and α-synuclein have each been localised in Aβ plaques in AD and in Lewy bodies in Parkinson's disease (PD) post-mortem brain tissues, respectively.[34–37] This raises the question of whether dityrosine cross-linking is present on human-derived tau assemblies. Using TEM immunogold labelling and fluorescence spectroscopy, we show that dityrosine cross-linking is observed on human AD tau oligomers and PHFs, and dityrosine colocalises with tau on NFTs in AD. However, using MCO of dGAE in vitro, we showed that prefibrillar tau assemblies are more amenable to dityrosine cross-linking than fibrils, suggesting that dityrosine crosslinking *in vivo* may have a different impact on the tau assemblies and activity. Nonetheless, dityrosine formation results in heat and SDS stability of oxidised prefibrillar and fibrillar tau assemblies, suggesting a general role of dityrosine crosslinking in enhancing pathological tau stability.

Results

Dityrosine crosslinking is observed in pathological tau from AD samples

We have previously shown the presence of dityrosine crosslinks in AD amyloid plaques.[36] Here, we first conducted immunogold labelling TEM on AD brain sections to investigate the presence of dityrosine crosslinks on pathological tau. The labelling of AD brain sections revealed densely packed tau-containing filaments, many showing the characteristic paired-helical appearance upon close inspection (Figure 1(A)). These filaments also labelled with an anti-dityrosine antibody, indicating the presence of dityrosine crosslinks. Since PHFs were not found in the age-matched control brain sections, only the data from the AD patients is shown in Figure 1(A). Very low immunogold labelling levels were observed for age matched controls (Figure S2).

Ex-vivo derived AD tau filaments[25] were also examined using immunogold TEM. Electron micrographs show the labelling of anti-dityrosine on the tau filaments supporting the view that the tau protein is cross-linked within the filaments (Figure 1 (B)). To examine whether dityrosine crosslinks occur earlier in the assembly process, AD brain-derived oligomers[38–39] were labelled with dityrosine antibody using single immunogold labelling, and these show the distinctive gold labels suggesting that dityrosine is also found within these earlier oli-

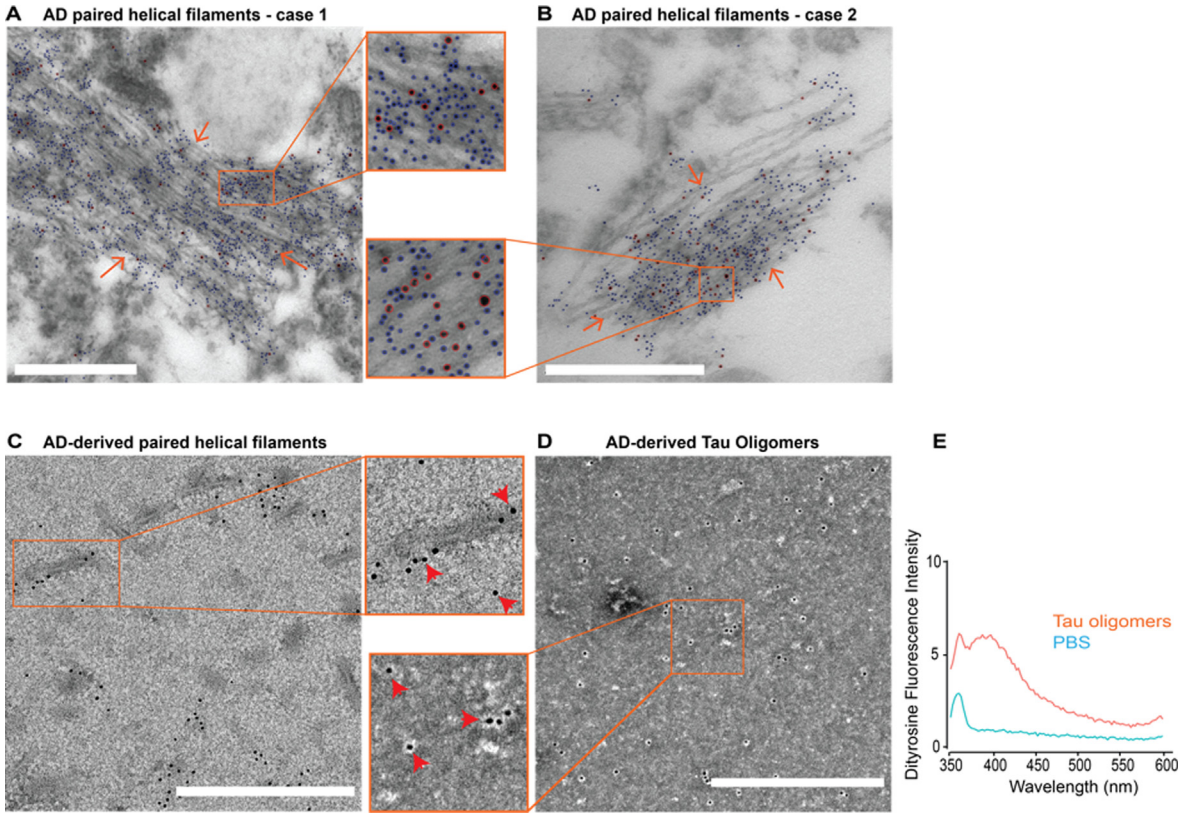

Figure 1. Dityrosine detection in AD-derived Tau species. (A) TEM double immunogold labelling revealed close, dense labelling of PHFs (orange arrow) using anti-dityrosine mouse monoclonal antibody (secondary gold conjugated anti-mouse 10 nm) and anti-tau rabbit polyclonal antibody (secondary gold conjugated anti-rabbit 5 nm) on AD brain sections showing neurofibrillary tangles (A & B, see Inserts: blue circles for tau and red circles for dityrosine). Orange Or arrows highlight PHF. **(C)** TEM single immunogold labelling revealed labelling of anti-dityrosine mouse monoclonal antibody on ex-vivo AD tissue-derived paired helical filaments (Insert: red arrows for dityrosine). **(D)** TEM single immunogold labelling revealed anti-dityrosine mouse monoclonal antibody labelling on ex-vivo AD-derived tau oligomers. (**E**) Dityrosine signal was confirmed for the AD-derived tau oligomers (red trace) with a fluorimeter using fluorescent excitation/emission 320 nm/340 – 600 nm, with dityrosine peak signal observed between 400–420 nm. Phosphate buffer (greencyan trace). Scale bar = 500 nm.

gomeric species (Figure 1(C)). In support of the presence of dityrosine crosslinks within brain derived oligomeric tau, a fluorescence emission peak was observed for the oligomeric species in solution at 410 nm, characteristic of the presence of dityrosine (Figure 1(D)).[28,36,40] Together, these data reveal that dityrosine crosslinks appear in both tau oligomers and fibrils in vivo and ex-vivo, suggesting a potentially important role for dityrosine in tau assembly and neurofibrillary tangle accumulation in AD.

Soluble and prefibrillar dGAE are more amenable to dityrosine crosslinking and its impact than fibrillar dGAE assemblies

To further examine the potential effects of dityrosine crosslinking on fibrillar tau, we examined the labelling of filaments formed from dGAE, which has been shown to form PHFs and SFs without additives.[24,26–27,41–42] Agitation of 300 μM dGAE for 6 h at 37° C resulted in the formation of a mixture of oligomeric and pre-fibrillar species, while incubation for 48 h resulted in mature filaments with a pronounced twist and some lateral bundling (Figure 2(A), (B), (C)).

We have shown that metal-catalysed oxidation (MCO) using Cu^{2+} and H_2O_2 results in dityrosine crosslinking of the dGAE.[23] In vivo, reactive oxygen species are produced from hydrogen peroxide catalysed by a metal ion such as Cu^{2+} via the Fenton reaction and Harber-Weiss cycle. This results in production of tyrosyl radical formation, isomeration and finally enolation.[34] In this study, soluble, pre-fibrillar and fibrillar dGAE samples (50 μM) were prepared from their respective stock preparations (Figure 2). The 50 μM soluble, pre-fibrillar and fibrillar forms of dGAE were incubated for 15 mins or 48 h under MCO conditions using Cu^{2+} and H_2O_2 to induce the formation of dityrosine crosslinks. The tyrosine and dityrosine levels within the samples were evaluated together by fluorescence

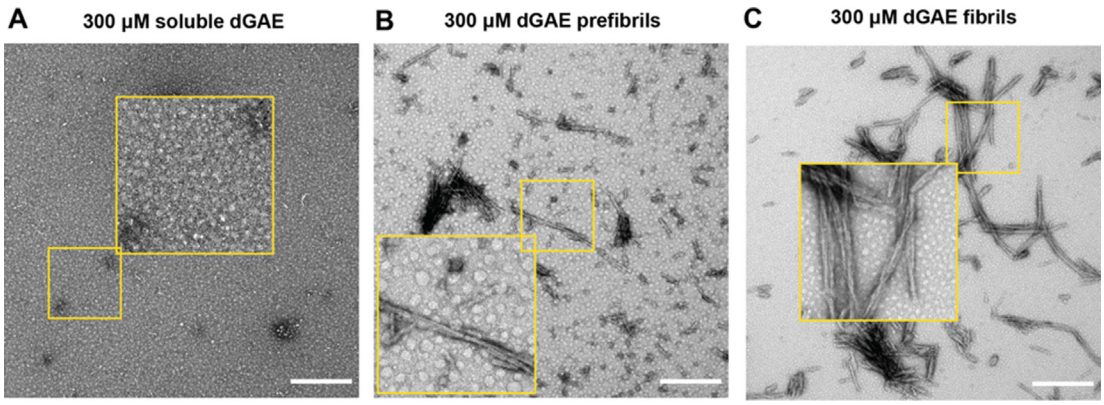

Figure 2. Preparation of dGAE assemblies for oxidation experiments. dGAE assemblies (300 μM) were prepared freshly (**A**), and incubated at 37 °C with agitation at 700 RPM for 6 h **(B)** or 48 h **(C)**. TEM imaging for the freshly prepared sample revealed small, round assemblies, described here as soluble species (**A**). The samples incubated for 6 h revealed short fibrils and small round assemblies, described here as prefibrils (**B**). Samples incubated for 48 h revealed long twisted and bundled fibrils described here as fibrils (**C**). Scale bar = 500 nm.

spectroscopy using an excitation wavelength of 280 nm for tyrosine and excitation of 310 nm for dityrosine (Figure 3(A)-(D)). A small peak is observed at 360 nm which arises due to a Raman scattering effect from the water in phosphate buffer. Soluble dGAE shows a strong tyrosine fluorescence signal which is reduced substantially following a 15 min incubation in oxidising conditions (Figure 3(A)), with the concurrent increase in the dityrosine signal at 410–420 nm (Figure 3(B)). Similarly, prefibrils showed a transition to dityrosine fluorescence following oxidation (Figure 3(A)-(B)). The level of dityrosine signal in the soluble and prefibrillar dGAE samples remained similar between 15 min and 48 h suggesting that the formation of dityrosine is rapid (Figure 3(B) & (D)). In contrast, mature fibrillar dGAE showed an extremely low dityrosine signal at 15 min, which remained similar at 48 h (Figure (B) & (D)), suggesting that fibrils are less susceptible to dityrosine crosslinking. The tyrosine signal decreases further from 15 min to 48 h incubation for all samples. For unoxidized samples, this may be due to lateral association of fibrils with time leading to the burial of the tyrosine. Indeed, tyrosine signal for unoxidised fibrils remains constant between 15 min and 48 h time point. For oxidised samples, this is due to a transition to dityrosine. Together, this reveals that soluble and prefibrillar dGAE assemblies are more amenable to dityrosine crosslinking than fibrillar species.

In order to examine the amyloid-fibrillar nature of the dGAE samples, Thioflavine S (ThS) fluorescence assays were conducted. ThS is similar to Thioflavine T and commonly used for tau assembly assays.[24] ThS fluorescence intensity increased only following 48 h incubation in the unoxidised soluble and prefibrillar dGAE assemblies (Figure 3(E)-(F)) and no significant increase in the fluorescence intensity was observed in the oxidised samples. Both these observations are consistent with previous results whereby oxidation appears to halt further self-assembly.[23] A minor increase in ThS fluorescence intensity was observed in the 48 h unoxidised fibrils compared to the same samples incubated for 15 min (Figure G). However, unlike the oxidised soluble and prefibrillar dGAE assemblies, oxidised dGAE fibrils showed increased ThS fluorescence intensity at 48 h when compared to the 15 min signal, suggesting that the fibrils still retain some ability to assemble further, which may arise from their reduced susceptibility to crosslinking following oxidation.

To investigate the secondary structure of the assemblies, circular dichroism spectroscopy (CD) was conducted (Figure 3(H)-(J)). CD for unoxidized soluble and prefibrillar species appear to show random coil signal after 15 mins but after 48 h incubation a low intensity signal was observed which may be due to decreased solubility as fibrils grow. However, both soluble and prefibrillar oxidised samples show very strong random coil signal arising from soluble, random coil dGAE in solution which changes only slightly in intensity from 15 mins to 48 h incubation. CD spectra for fibril samples show the expected β-sheet signal for the unoxidized fibrils sample which increases with time, but the decreased intensity β-sheet signal for the oxidised sample may a further decrease in solubility upon oxidation. This seems to suggest that changes happen rapidly and there is little further conformational change after 15 mins incubation following oxidation and dityrosine crosslinking.

The appearance of soluble, prefibrillar and fibrillar samples of dGAE that had been oxidised for 15 mins only or remained unoxidised were compared using TEM. TEM is qualitative method rather than quantitative and images shown are representative of what was observed on the grids. As expected, the electron micrographs of unoxidised dGAE

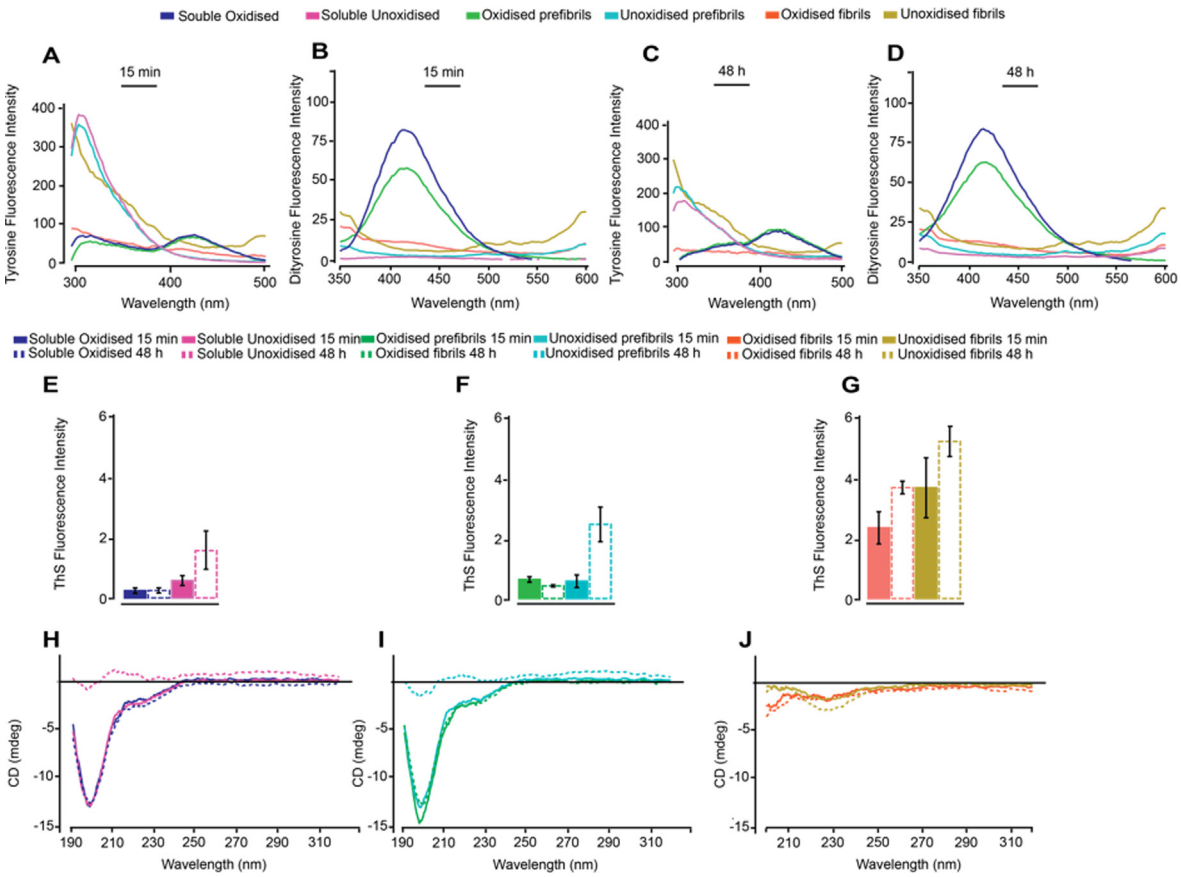

Figure 3. Self-assembly properties and conformation of oxidised dGAE assemblies. Soluble, prefibrils and fibrils of dGAE (50 μM) were prepared from their respective stock assemblies, left unoxidised or oxidised using $CuCl_2$: dGAE at 10:1 ratio, then mixed with 2.5 mM H_2O_2 and incubated for 15 min or 48 h at 37 °C/700 rpm. Tyrosine signal was monitored using an excitation/emission 280 nm/290 – 500 nm, with peak tyrosine signal observed at 305 nm. While dityrosine signal was collected using fluorescent excitation/emission 320 nm/340 – 600 nm, with dityrosine peak signal observed between 400–420 nm. Tyrosine signal collected at 15 min incubation shows reduction in intensity for all the oxidised samples compared to unoxidized samples (**A**). Fluorescence reading showed a high intensity signal for dityrosine formation in oxidised soluble assemblies, with lower intensity observed for prefibrils and even lower signal for fibrils. Unoxidised samples showed no peak at 420 nm for dityrosine (**B**). Tyrosine signal at 48 h decreased further in all oxidised samples and a minor reduction was observed in the unoxidised samples compared to signals collected at 15 min (**C**). Dityrosine signal remained similar to the signal observed at 15 min signal for oxidised assemblies (**D**). ThS fluorescence assay was conducted to observe the degree of self-assembly using excitation/emission of 440/460–600. Soluble (**E**) prefibrillar (**F**) and fibrillar (**G**) unoxidised dGAE assemblies showed increased ThS fluorescence at 48 h compared to 15 min; while oxidised samples remained similar between the time points. Circular dichroism (CD) spectroscopy for all the soluble assemblies except soluble unoxidised samples at 48 h revealed a typical random coil signal (**H**). All dGAE prefibrils except the unoxidised prefibrils at 48 h, also showed random coil signal, however to a lower extent in unoxidised prefibrils at 15 min and oxidised prefibrils at 48 h (**I**). CD showed the absence of random coiled conformation in unoxidised and oxidised fibrils and the appearance of β-sheet, especially in unoxidised fibrils at 48 h indicated by the presence of a minimum at 228 nm (**J**).

samples showed very small particles for soluble dGAE, short fibrils for prefibrillar and longer fibrils for those categorised as fibrils (Figure 4(A)-(F)). In contrast soluble (Figure A and B) and prefibrillar (Figure C and D) samples appeared to form small and larger rounded structures following oxidising incubation, suggesting that the oxidation of amino acid residues, including tyrosine to form dityrosine resulted in the prevention of further elongation and formation of trapped, relatively stable spherical species. However, the fibrillar sample remains fibrillar and their morphology changed very little compared to the unoxidised samples. Some lateral association of fibrils was apparent, and this may arise from crosslinking between fibres (Figure E and F).

After 48 h incubation, all three samples incubated under unoxidised conditions had assembled to some extent with either very long fibrils, or shorter fibres in the soluble dGAE sample (Figure 4 E-F).

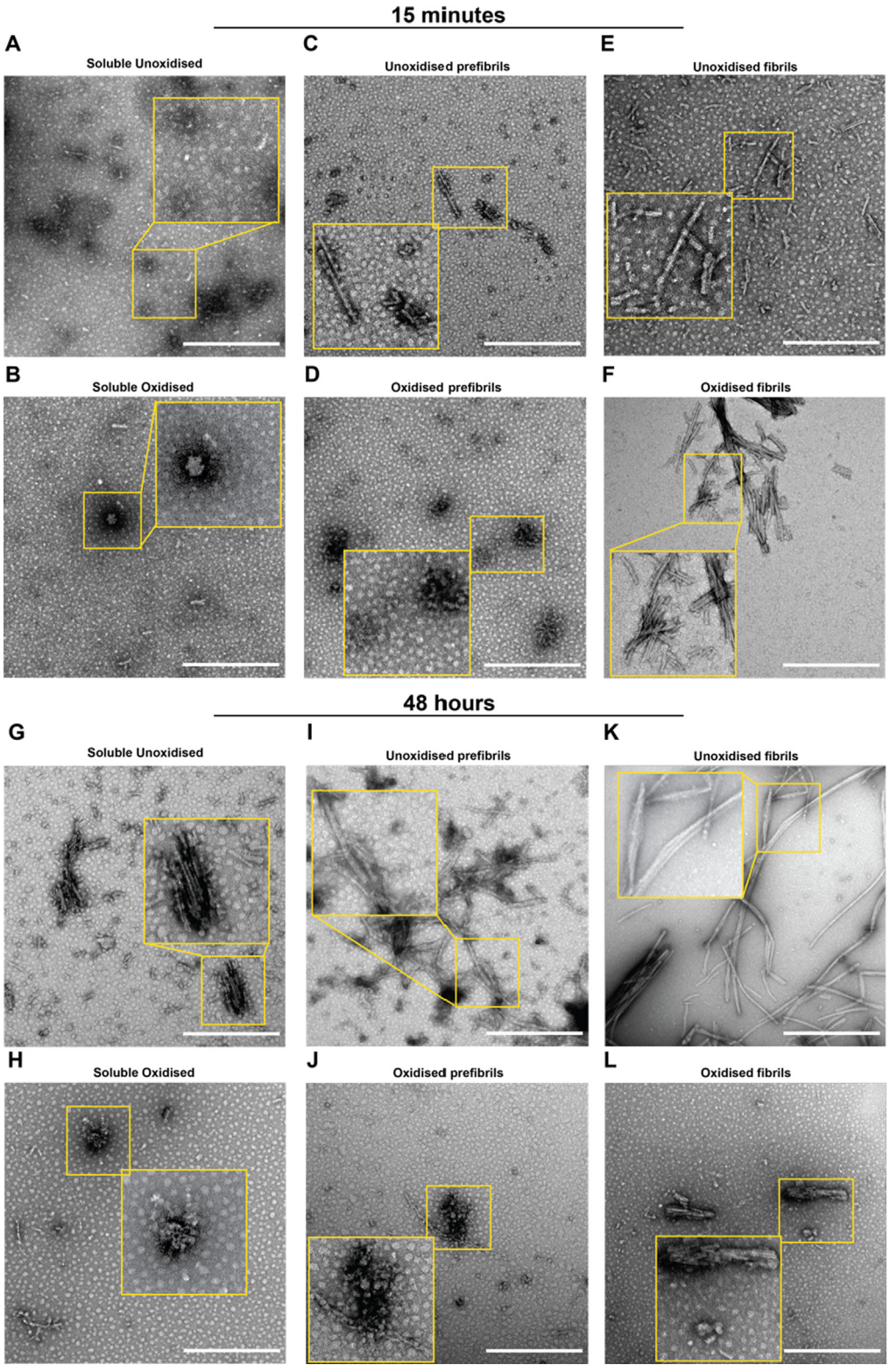
15 minutes
A
Soluble Unoxidised
C
Unoxidised prefibrils
E
Unoxidised fibrils
B
Soluble Oxidised
D
Oxidised prefibrils
F
Oxidised fibrils
48 hours
G
Soluble Unoxidised
I
Unoxidised prefibrils
K
Unoxidised fibrils
H
Soluble Oxidised
J
Oxidised prefibrils
L
Oxidised fibrils

In comparison, after incubation in oxidising conditions, the soluble and prefibrillar samples showed mostly trapped, spherical species (similar to those found at 15 mins incubation) but with some short fibrillar protofibrils (narrower elongated fibrils). The fibrillar sample showed shortening of the fibrils, suggestive of fragmentation or breakage of the stabilised fibres, or prevention of elongation, with more obvious lateral association than observed after 15 mins incubation. This may indicate that these cross-linked stabilised fibres are susceptible to breakage during incubation with shaking.

To investigate the apparent stability caused by the dityrosine crosslinking further, we investigated the heat and SDS insolubility of the oxidised and unoxidised samples (Figure 5(A)). The samples were boiled at 100 °C in Laemmli sample buffer containing 4.4% LDS and 10% β-mercaptoethanol and then resolved by SDS–PAGE electrophoresis and stained with Coomassie brilliant blue.[29] Unoxidised soluble dGAE sample mainly separated as a monomer (10/12 kDa) while prefibrillar and fibrillar samples show the appearance of a dimer (20 kDa/24 kDa). Insoluble species are found in the well and are most clearly evident in the fibril sample as expected. For the oxidised samples, there is a clear increase in the protein material in the well for each soluble, prefibrillar and fibril sample compared to the unoxidised and a dimer appears in all three samples. The fibril sample also shows some higher molecular weight species which suggests the stabilisation of larger species potentially via dityrosine as well as other surface interactions. The structure of paired helical filaments consists of two protofilaments with two tau molecules associated so that tyrosines can participate in dityrosine on both sides of the filament. Furthermore, each protofilament contains multiple tyrosines.

This shows that 15 mins oxidation alone results in heat and SDS insolubility of the soluble, prefibrillar and fibrillar assemblies. This is more pronounced in the fibrillar sample, which indicated that heating and incubation in the Laemmli buffer resulted in the dissociation of the majority of the unoxidised fibrils to monomers and multimers. However, the oxidised samples that were treated the same way showed assemblies that remained as monomers, multimers, and some were too large and would have failed to enter the gel (≥250 kD, red arrows). This suggests that the oxidised assemblies maybe stabilised through dityrosine formation. Comparison of heat and SDS denatured (fully denatured) with SDS only (partially denatured) showed that non-oxidised fibrils run as a dimer with staining in the well from insoluble (presumably fibrillar) material, while the fully denatured condition leads to monomer with low well staining (Figure S3). In contrast, while oxidised fibrils also run as dimer and monomer in partially and fully denatured respectively, they show staining in the well under both conditions and the monomer and dimer bands are weak intensity. This supports the view that oxidation leads to increased resistance to denaturation.

dGAE contains a single cysteine residue at residue 322. To examine whether the oxidation of cysteine plays a role in the conformational and morphological changes in dGAE upon oxidation, the ability of C322A variant dGAE to form dityrosine was investigated and compared with a control dGAE with a Y310A substitution. Oxidised wildtype dGAE shows a strong signal from dityrosine at 410-420 nm as previously shown, and this remains clearly observed for C322A dGAE with a similar intensity as wildtype (Figure 5(B)-(C)). As expected, however, this signal is not observed for Y310F since this variant does not include a tyrosine residue. ThS fluorescence shows that wildtype dGAE and C322A dGAE assemble over 48 h only when incubated under non-oxidising conditions, while Y310F appears to be unable to self-assemble under either oxidising or non-oxidising conditions used in this study (Figure 5(E)-(G)). Collectively these data showed that cysteine is not involved in the dGAE stabilisation following oxidation, while tyrosine appears to be involved in dGAE assembly.

Discussion

Dityrosine occurs naturally in proteins, helping to increase their stability. This modification has been found in many elastic and structural proteins, including elastin, fibroin, keratin, cuticlin, and

Figure 4. Morphologies of unoxidised and oxidised assemblies. Soluble, prefibrils and fibrils of dGAE (50 μM) were prepared from their respective stock assemblies, incubated unoxidised or oxidised using $CuCl_2$:dGAE at 10:1 ratio, then mixed with 2.5 mM H_2O_2 and left for 15 min or 48 h at 37 °C/700 RPM. Compared to the unoxidised soluble assemblies, oxidised soluble assemblies showed larger round assemblies at 15 mins (**A1-A2)**. Similarly, compared to the unoxidised prefibrils, oxidised prefibrils showed mostly large amorphous assemblies comprised of inter-connected smaller assemblies at 15 mins (**B1-B2**). Compared to unoxidised fibrils, oxidised fibrils showed many laterally connected fibrils at 15 min (**C1-C2**). The soluble unoxidised assemblies formed short fibrils at 48 h (**D1**), while the soluble oxidised assemblies formed large round assemblies (**D2)**. Similarly, unoxidised prefiibrils showed long, mature fibrils at 48 h (**E1**), while the oxidised prefibrils formed large round assemblies (**E2**). Unoxidised fibrils showed longer, matured fibrils (**F1**), while the oxidised fibrils revealed short, blunt morphology at 48 h (**F2**). Scale bar = 500 nm.

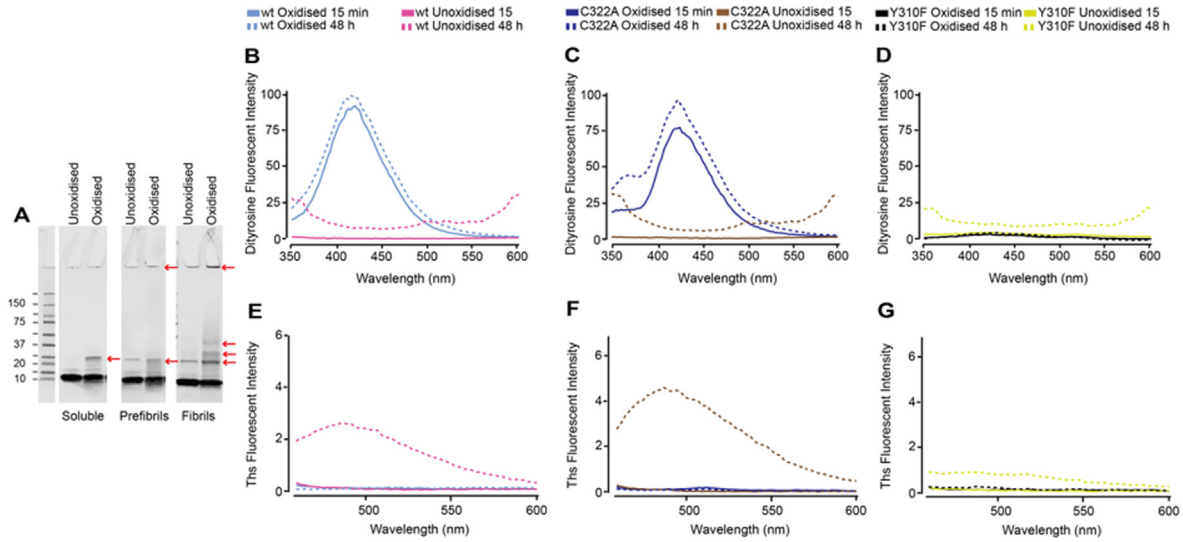

Figure 5. Stability of crosslinked assemblies, dityrosine formation susceptibility and self-assembly in dGAE variants. Soluble, prefibrils and fibrils of dGAE (50 μM) were prepared from their respective stock assemblies, left unoxidised or oxidised using $CuCl_2$:dGAE at 10:1 ratio, then mixed with 2.5 mM H_2O_2 and left for 15 min at 37 °C/700 rpm. Compared to all unoxidised assemblies, the oxidised assemblies showed heat and SDS insolubility that is more pronounced in the fibril sample (**A**). 50 μM soluble wild-type dGAE, dGAE with C322A substitution and dGAE with Y310F substitution were prepared, left unoxidised or oxidised using $CuCl_2$:dGAE at 10:1 ratio then mixed with 2.5 mM H_2O_2 and left for 15 min or 48 h at 37 °C/700 rpm. Fluorescence readings showed an increase in intensity signal for dityrosine in oxidised wildtype dGAE (**B**) and C322A dGAE (**C**) samples at 15 min and 48 h. No dityrosine signal was detected in Y310F dGAE sample (**D**). Unoxidised wildtype dGAE (**E**) and C322A dGAE (**F**) assemblies incubated for 48 h showed increased ThS fluorescence suggesting assembly, while Y310F dGAE showed no self-assembly (**G**). In contrast, oxidised samples showed no ThS fluorescence suggesting prevention of assembly.

collagen,[43–46] where it is believed to increase their mechanical strength and subsequently their insolubility.[47] However, the formation of dityrosine in proteins is also implicated in many diseases, including AD, and PD,[36–37,40,48] cystic fibrosis,[49] atherosclerosis,[50] cataracts in the eye lens[51–52] and acute myocardial infarction.[53] Our previous work has co-localised dityrosine with Aβ within Aβ plaques[36] and Lewy bodies with α-synuclein,[35,37] suggesting that it could play a role in increasing the insolubility of Aβ plaques in AD and α-synuclein aggregates in PD. It remained to be determined whether dityrosine crosslinking is formed in the tau aggregates in human AD brains. Here, we have revealed that dityrosine forms *in vivo* on tau oligomers and filaments within NFTs both in situ in brain and also localised to ex-vivo AD-derived assemblies. Using the PHF-core tau fragment (dGAE) as a model, which forms dityrosine cross-links via tyrosine 310, we also showed that although dityrosine forms on tau assemblies, mature fibrillar species are less amenable to dityrosine crosslinking and that dityrosine formation promotes heat and SDS insolubility of the tau aggregates.

It is known that exposure to reactive oxygen species (ROS), ageing, nitrogen dioxide, metal ions and lipid hydroperoxides can result in dityrosine formation.[40,54–56] Oxidative stress accumulates early in AD, increasing with disease pathology.[57–58] ROS, ageing, metal ions and other factors could induce dityrosine crosslinking on the tau oligomers and fibrils *in vivo*. Dityrosine crosslinking on tau fibrils could increase their stability and insolubility. The PHFs extracted from the AD brain are highly insoluble and resistant to proteolytic cleavage. Specifically, the early-stage PHF-tau has reduced SDS solubility,[31,59] while late-stage PHF tau exhibits SDS and sarcosyl insolubility.[30–32] Previous work on full-length tau aggregation with arachidonic acid showed that dityrosine crosslinked tau fibrils have increased SDS stability, suggesting that the crosslinking may play a role in stabilising the early-stage PHFs and confers stability to convert into late-stage PHFs.[29] Here, we find that the oxidised dGAE fibrils are difficult to resuspend in solution, are heat and SDS-insoluble and remained strongly laterally associated to one another, shown by TEM. Given that we find dityrosine crosslinking on AD-derived tau fibrils and in NFTs, this finding suggests that this post-translational modification increases the insolubility of tau fibrils and NFTs in AD.

By comparing the capability of soluble, prefibrillar and fibrillar dGAE to form dityrosine, our findings indicate that fibrillar tau assemblies are less amenable to dityrosine crosslinking. This is evidenced by the very low fluorescence signal observed in the oxidised fibrillar dGAE samples in

spectroscopic experiments, unlike in the oxidised soluble and prefibrillar assemblies, which showed robust dityrosine formation. This apparent inability to form dityrosine compared to soluble and prefibrillar assemblies could be due to the inaccessibility to the tyrosine residue on the tau molecule when it is arranged in a fibrillar architecture. The only tyrosine present in dGAE is at position 310, which is buried within the PHF core in the Cryo-EM structures of tau filaments from many tauopathies, including AD and CTE[21,25,27,60–61] (example Figure S1). Recent Cryo-EM evidence indicates that the dGAE forms a similar structure as that of AD and CTE.[27] Therefore, it can be concluded that the decreased ability of dGAE fibrils to form dityrosine under MCO conditions is due to the inaccessibility of the tyrosine residue, unlike in the soluble and prefibrillar dGAE assemblies.

Our *in vitro* work on dGAE and Aβ both suggest that dityrosine formation traps the assemblies in a conformation that doesn't favour further elongation into fibrils.[23,28] However, whether dityrosine crosslinked tau oligomers also fail to elongate to fibrils *in vivo* is a question of future research. We have shown that dityrosine crosslinked tau oligomers are not toxic to human neuroblastoma cells even after three days in culture[23] although we also find that dGAE is generally non-toxic in its oligomeric form.[41] We have also shown that dityrosine does appear to be associated with neurofibrillary tangle in AD tissue and extracted species. However, the stage at which dityrosine formation occurs during the assembly and deposition of tau remains to be elucidated. It is unclear at the moment what the impact of dityrosine crosslinking is on the aggregation and toxicity of tau oligomers *in vivo*. Nonetheless, it is essential to highlight that the influence of dityrosine on tau aggregation and toxicity may depend on the extent of the dityrosine crosslinking.[23] A highly crosslinked protein may be highly trapped and exhibit a different property than a partially crosslinked protein. This, therefore, makes it impossible to speculate a general model of the influence of this modification on tau and indeed other proteins like Aβ.

Finally, cysteine oxidation can be induced by oxidative stress conditions and is known to influence the functions, properties and toxicity of tau.[62–64] dGAE has a single cysteine residue at position 322, and we have previously shown that it forms PHFs independent of this cysteine and that assembly is enhanced under reducing conditions or using C322A variant.[24,65] To examine whether the oxidation of cysteine plays a role in the conformational and morphological changes in dGAE upon oxidation, we utilised dGAE C322A. This revealed that cysteine oxidation is not involved in stabilising the tau aggregates; instead, the effects observed resulted from dityrosine crosslinking. However, this does not rule out the involvement of other oxidative modifications, such as the oxidation of histidine and phenylalanine, which are all present in dGAE. Future studies would delineate the specific amino acids involved. Nonetheless, the immunogold labelling experiments on AD brain tissue and AD-derived fibrils and oligomers strongly suggest that dityrosine crosslinking has *in vivo* relevance to tau in AD, similar to its role on Aβ[36] and α-synuclein[35,37] in AD and PD, respectively. Given the role of dityrosine in increasing the mechanical strength and insolubility of proteins,[47] we believe that its association with hallmarks of AD (tau and Aβ) and PD (α-synuclein) that are known to be insoluble in these diseases, could suggest its participation in promoting the insolubility, accumulation and resistance to degradation of NFTs and Aβ plaques in AD and α-synuclein aggregates in Lewy bodies in PD.

In conclusion, for the first time, our findings showed that, similar to Aβ plaques and α-synuclein Lewy bodies, dityrosine crosslinks PHFs in AD and is a posttranslational modification of AD-derived tau oligomers and fibrils. Our finding suggests that the assembly state of the tau molecule will influence its ability to be crosslinked, such that, when the tyrosine is buried in the case of fibrils, it becomes less amenable to dityrosine formation. This finding has implications for understanding the mechanism governing the insolubility and toxicity of tau assemblies *in vivo* and providing therapeutic avenues that focus on the tau molecule.

Materials and Methods

Cases

Tissue from the middle--frontal gyrus of three AD subjects and one age-matched control were used for transmission electron microscope (TEM) immunogold labelling. The samples were obtained from the London Neurodegenerative Disease Brain Bank with informed consent and under material transfer agreement and stored at −80 °C under local ethics committee guidelines (Table 1).

Immunogold labelling for total tau and dityrosine

The brain sections were labelled using our established method of immunogold labelling.[36] Phosphate-buffered saline (pH 8.2) containing 1% BSA, 500 μl/l Tween-20, 10 mM Na EDTA, and 0.2 g/l NaN3 (henceforth called PBS+), was used throughout. Briefly, thin brain sections were mounted on TEM grids and blocked for 30 minutes in normal goat serum (1:10 dilution), labelled with 10 μg/ml IgG anti-tau rabbit polyclonal antibody (Sigma, SAB4501831) and 10 μg/ml IgG anti-dityrosine mouse monoclonal antibody (JaICA, Shizuoka, Japan), and left in a humid container overnight at room temperature. The sections were rinsed in PBS + three times for 2 minutes and

Table 1 Characteristics of subjects provided by London Neurodegenerative Diseases Brain Bank.

Case	Age	Sex	Post-mortem delay (h)	Pathological diagnosis
AD 1	77	F	42	Alzheimer's disease (modified Braak stage 5)
AD 2	93	F	38	Alzheimer's disease--tau stage 6 with moderate angiopathy
AD 3	68	M	25	Alzheimer's disease -tau stage 6 with moderate angiopathy
Control	80	F	3	Control – minimal age-related changes

immunogold labelled with goat anti-mouse 10 nm and goat anti-rabbit 5 nm for 1 hour (1:10 dilution). Then the grids were rinsed three times for 10 minutes with PBS+, followed by four 5-minute rinses in distilled water, before post-staining in 0.05% aqueous uranyl acetate for 1 hour. Ex-vivo PHFs and tau oligomers were provided by Michel Goedert and Rayez Kayed groups, respectively. These samples have been well-characterised by both groups.[25,38–39]

For the single labelling of ex-vivo PHFs and tau oligomers with dityrosine antibody, 4 μL of each sample were placed onto 400-mesh carbon-coated grids (Agar Scientific, Essex, UK), allowed to adhere for 1 min, and the excess sample removed using filter paper. The grids were blocked using normal goat serum (1:10 in PBS +) for 15 min, then incubated with mouse anti-dityrosine monoclonal antibody (10 μg/ml IgG; JaICA, Shizuoka, Japan) for 2 h at room temperature. The grids were rinsed three times for 2 min in PBS+, and then labelled with a 10-nm gold particle-conjugated goat anti-mouse IgG secondary probe (GaM10 British BioCell International, Cardiff, UK; 1:10 dilution) for 1 h at room temperature. The grids were rinsed five times for 2 min using PBS+, five times for 2 min with distilled water, then negatively stained as described below.

Negative-stain transmission electron microscopy (TEM)

Samples (4 μL) were placed on 400-mesh carbon-coated grids (Agar Scientific, Essex, UK) and incubated for 1 min. The excess sample was blotted using filter paper, and the grids were washed with 4 μL filtered milli-Q water. The grids were then negatively stained for 40 sec using 4 μL of filtered 2% (w/v) uranyl acetate. The excess stain was blotted with filter paper and grids left to air-dry before storage. TEM projection images were collected using a JEOL JEM1400-Plus Transmission Electron Microscope operated at 80 kV equipped with a Gatan OneView camera (4k × 4k).

Preparation and assembly of dGAE

Recombinant wild-type and variant dGAE were prepared using our established method.[24] The dGAE was expressed in *Escherichia coli* and purified by P11 phosphocellulose chromatography following heat treatment. The protein fractions were eluted with 50 mM PIPES buffer (pH 6.8) or 50 mM MES buffer (pH 6.25), both supplemented with 1 mM EGTA, 5 mM EDTA, 0.2 mM $MgCl_2$ and 5 mM 2-mercaptoethanol containing 0.1–1 M KCl. The peak of protein elution was identified by protein assay (at 0.3–0.5 M KCl) and dialyzed against 80 mM PIPES buffer (pH 6.8), 1 mM EGTA, 5 mM EDTA, 0.2 mM $MgCl_2$, 5 mM 2-mercaptoethanol, or PB (10 mM; pH 7.4). The dGAE protein concentration was measured using Advanced Protein Assay Reagent (Cytoskeleton, Inc.) with bovine serum albumin as a standard. dGAE was finally diluted with 10 mM phosphate buffer (pH 7.4). dGAE (300 μM) was prepared in phosphate buffer (10 mM; pH7.4) and incubated in the dark for i) 0 minutes; ii) 6 hours; or iii) 48 hours at 37 °C with shaking at 700 rpm using a thermomixer C (Eppendorf, Germany). Based on TEM observations, henceforth, the samples will be referred to as (i) soluble dGAE; (ii) prefibrillar dGAE; and (iii) fibrillar dGAE, respectively.

Metal-catalysed oxidation of dGAE

The soluble, prefibrillar and fibrillar dGAE samples were diluted to 50 μM before being used for metal-catalysed oxidation. For the fibrillar samples, 50 μM of the fibrils were obtained by first determining the concentration of the fibrils. This was achieved by spinning the fibrillar dGAE for 30 minutes at 20,000 g to separate the supernatant (containing unaggregated, soluble dGAE) and pellet (containing fibrils). The concentration of the soluble dGAE in the supernatant was used to back-calculate the concentration of dGAE in the fibrils. Soluble, prefibrillar and fibrillar dGAE (at 50 μM) were incubated in phosphate buffer (10 mM; pH7.4) alone (unoxidised) or in the presence of 500 μM $CuCl_2$ (peptide: $CuCl_2$ ratio 1:10) and 2.5 mM H_2O_2 (oxidised) and incubated for 15 minutes or 48 hours at 37 °C with shaking at 700 rpm. The oxidation reaction was quenched by adding 2 mM EDTA to the assembly mixture. Oxidation of variant dGAE (carrying the mutations C322A and Y310F) was done using the same procedure. A minimum of three independent experiments were conducted to ensure the reproducibility of the findings.

Fluorescence spectroscopy

Dityrosine formation was monitored using a fluorescent excitation wavelength of 320 and emission collected between 340 – 600 nm, with

dityrosine peak signal expected between 400–420 nm,[24] using a fluorescence spectrophotometer (Varian ltd., Oxford, UK) and a 1-cm path length quartz cuvette (Starna, Essex, UK). The tyrosine fluorescence signal was monitored using an excitation wavelength of 280 nm and emission between 290 – 600, with the peak tyrosine emission observed at 305 nm. For all the measurements, the excitation and emission slits were set to 10 nm with a scan rate set to 300 nm/min with 2.5 nm data intervals and an averaging time of 0.5 s. The photomultiplier tube detector voltage was set at 500 V.

Thioflavin s (ThS) fluorescence assay

To assess the assembly of dGAE in the different samples, a portion (10 μL) of each was incubated for 3 min with ThS (5 μM in 20 mM MOPs buffer, pH 6.8). ThS fluorescence intensity was observed using a fluorescence spectrophotometer (Varian ltd., Oxford, UK) and a 1-cm path length quartz cuvette (Starna, Essex, UK). The excitation wavelength was set at 440 nm, with emission between 460 to 600 nm collected, with the peak emission observed at 483 nm. Each experiment included a minimum of three independent experiments. The peak emission was collected and analysed, then plotted graphically.

Circular dichroism (CD)

The secondary structure of the samples was assessed using the Jasco J715 CD spectrometer (Jasco, Goh-Umstadt, Germany). Each sample (40 μL) was placed into a 0.2-mm path length quartz cuvette (Hellma) and scanned between 190 and 260 nm. The CD spectra were collected in triplicate at a temperature of 21 °C.

SDS-PAGE and immunoblotting

dGAE samples (20 μL) for each condition were mixed with 4x Laemmli sample buffer (containing 4.4% LDS) (Bio-Rad), supplemented with 10% 2-mercaptoethanol, boiled for 10 min at 100 °C, resolved using a 4%–20% gradient Mini-Protean® TGX Precast Gels (Bio-Rad) at 100 V until the sample buffer reached the end of the gel. Partial denatured samples were mixed only with 4x Laemmli buffer but were not boiled and no 2-mercaptoethanol was used. The gels were stained using Coomassie Blue stain. Images were collected using LI-COR Odyssey XF.

Author contributions

M.B.M. planned and carried out the work; Y.K.A.-H., SO, TK, LB, KM and J.E.R. contributed experimental work. M.B.M. and L.C.S. wrote the paper; Y.K.A.-H and G.B. edited the paper and provided training. GB, CRH and CMW reviewed and edited the paper. LCS managed the project.

CRediT authorship contribution statement

Mahmoud B. Maina: Conceptualization, Methodology, Investigation, Formal analysis, Writing – original draft. **Youssra K. Al-Hilaly:** Methodology, Investigation, Writing – review & editing. **Sebastian Oakley:** Investigation. **Gunashekar Burra:** Methodology. **Tahmida Khanon:** Investigation. **Luca Biasetti:** Investigation. **Kurtis Mengham:** Investigation. **Karen Marshall:** Investigation. **Charles R. Harrington:** Resources. **Claude M. Wischik:** Resources. **Louise C. Serpell:** Supervision, Writing – review & editing, Project administration, Funding acquisition.

Acknowledgements

The authors are grateful to M Goedert (MRC Laboratory of Molecular Biology, Cambridge, UK) for ex-vivo paired helical filaments which were kindly contributed by Bernandino Ghetti (Indiana University, USA). The authors are very grateful to Urmi Sengupta, Nemil Bhatt and Rakez Kayed (University of Texas, USA) for providing ex-vivo tau oligomers. TEM work was performed at the University of Sussex's Electron microscopy imaging centre (EMC), funded by the School of Life Sciences, the Wellcome Trust (095605/Z/11/A, 208348/Z/17/Z) and the RM Phillips Trust. The authors thank Dr Pascale Schellenberger for valuable support.

Funding

This work was supported by funding from Alzheimer's Society [AS-PG-16b-010] awarded to LCS and funding MBM. MBM is funded by the Alzheimer's Association. YA is supported by WisTa Laboratories Ltd (PAR1596). The work was supported by ARUK South Coast Network. GB was supported by European Molecular Biology Organisation (EMBO) Short-Term Fellowship award (EMBO-STF 7674). LCS is supported by BBSRC [BB/S003657/1]. Urmi Sengupta, Nemil Bhatt, Rakez Kayed acknowledge the funding that supports their contribution (NIH grants to R.K: R01 AG054025 and U24AG072458).

Conflicts of Interest

C.R.H. and C.M.W. hold Offices within TauRx Therapeutics Ltd. and are named inventors on patents in the field of tau protein in neurodegenerative disorders. The funding sponsors had no role in the design of the study; in the collection, analyses, or interpretation of data;

in the writing of the manuscript, and in the decision to publish the results. The remaining authors declare no conflicts of interest.

Data Sharing

No big data is generated from this work. The data generated and used to make figures in this manuscript will be available upon request.

Appendix A. Supplementary Data

Supplementary data to this article can be found online at https://doi.org/10.1016/j.jmb.2022.167785.

Received 29 May 2022;
Accepted 3 August 2022;
Available online 9 August 2022

Keywords:
Alzheimer's disease;
tau;
dityrosine;
paired helical filaments;
oxidative stress

References

1. Cleveland, D.W., Hwo, S.Y., Kirschner, M.W., (1977). Physical and chemical properties of purified tau factor and the role of tau in microtubule assembly. *J. Mol. Biol.* **116**, 227–247.
2. Weingarten, M.D., Lockwood, A.H., Hwo, S.Y., Kirschner, M.W., (1975). A protein factor essential for microtubule assembly. *PNAS* **72**, 1858–1862.
3. Maina, M.B., Bailey, L.J., Wagih, S., Biasetti, L., Pollack, S. J., Quinn, J.P., (2018). The involvement of tau in nucleolar transcription and the stress response. *Acta Neuropathol. Commun.* **6**, 70.
4. Sotiropoulos, I., Galas, M.C., Silva, J.M., Skoulakis, E., Wegmann, S., Maina, M.B., (2017). Atypical, non-standard functions of the microtubule associated Tau protein. *Acta Neuropathol. Commun.* **5**, 91.
5. Bukar Maina, M., Al-Hilaly, Y.K., Serpell, L.C., (2016). Nuclear Tau and Its Potential Role in Alzheimer's Disease. *Biomolecules.* **6**, 9.
6. Sultan, A., Nesslany, F., Violet, M., Begard, S., Loyens, A., Talahari, S., (2011). Nuclear tau, a key player in neuronal DNA protection. *J. Biol. Chem.* **286**, 4566–4575.
7. Grundke-Iqbal, I., Iqbal, K., Tung, Y.C., Quinlan, M., Wisniewski, H.M., Binder, L.I., (1986). Abnormal phosphorylation of the microtubule-associated protein tau (tau) in Alzheimer cytoskeletal pathology. *Proc. Natl. Acad. Sci. U S A.* **83**, 4913–4917.
8. Wischik, C.M., Novak, M., Thøgersen, H.C., Edwards, P. C., Runswick, M.J., Jakes, R., (1988). Isolation of a fragment of tau derived from the core of the paired helical filament of Alzheimer disease. *PNAS* **85**, 4506–4510.
9. Brion, J.P., Couck, A., Passareiro, E., Flament-Durand, J., (1985). Neurofibrillary tangles of Alzheimer's disease: an immunohistochemical study. *J. Submicroscopic Cytol.* **17**, 89–96.
10. Kosik, K.S., Joachim, C.L., Selkoe, D.J., (1986). Microtubule-associated protein tau (tau) is a major antigenic component of paired helical filaments in Alzheimer disease. *PNAS* **83**, 4044–4048.
11. Martin, L., Latypova, X., Terro, F., (2011). Post-translational modifications of tau protein: implications for Alzheimer's disease. *Neurochem. Int.* **58**, 458–471.
12. Oakley, S.S., Maina, M.B., Marshall, K.E., Al-Hilaly, Y.K., Harrington, C.R., Wischik, C.M., (2020). Tau Filament Self-Assembly and Structure: Tau as a Therapeutic Target. *Front. Neurol.* **11**
13. Alonso, A.C., Grundke-Iqbal, I., Iqbal, K., (1996). Alzheimer's disease hyperphosphorylated tau sequesters normal tau into tangles of filaments and disassembles microtubules. *Nat. Med.* **2**, 783–787.
14. Gamblin, T.C., Chen, F., Zambrano, A., Abraha, A., Lagalwar, S., Guillozet, A.L., (2003). Caspase cleavage of tau: linking amyloid and neurofibrillary tangles in Alzheimer's disease. *Proc. Natl. Acad. Sci. U S A.* **100**, 10032–10037.
15. Schweers, O., Mandelkow, E.M., Biernat, J., Mandelkow, E., (1995). Oxidation of cysteine-322 in the repeat domain of microtubule-associated protein tau controls the in vitro assembly of paired helical filaments. *Proc. Natl. Acad. Sci. U S A.* **92**, 8463–8467.
16. Reynolds, M.R., Berry, R.W., Binder, L.I., (2005). Site-specific nitration and oxidative dityrosine bridging of the tau protein by peroxynitrite: implications for Alzheimer's disease. *Biochemistry* **44**, 1690–1700.
17. Reynolds, M.R., Berry, R.W., Binder, L.I., (2005). Site-Specific Nitration Differentially Influences τ Assembly in Vitro. *Biochemistry* **44**, 13997–14009.
18. Ko, L.W., Ko, E.C., Nacharaju, P., Liu, W.K., Chang, E., Kenessey, A., (1999). An immunochemical study on tau glycation in paired helical filaments. *Brain Res.* **830**, 301–313.
19. Necula, M., Kuret, J., (2004). Pseudophosphorylation and Glycation of Tau Protein Enhance but Do Not Trigger Fibrillization in Vitro*. *J. Biol. Chem.* **279**, 49694–49703.
20. Lebouvier, T., Scales, T.M., Williamson, R., Noble, W., Duyckaerts, C., Hanger, D.P., (2009). The microtubule-associated protein tau is also phosphorylated on tyrosine. *J. Alzheimer's Dis. : JAD.* **18**, 1–9.
21. Ait-Bouziad, N., Chiki, A., Limorenko, G., Xiao, S., Eliezer, D., Lashuel, H.A., (2020). Phosphorylation of the overlooked tyrosine 310 regulates the structure, aggregation, and microtubule- and lipid-binding properties of Tau. *J. Biol. Chem.* **295**, 7905–7922.
22. Tremblay, M.A., Acker, C.M., Davies, P., (2010). Tau phosphorylated at tyrosine 394 is found in Alzheimer's disease tangles and can be a product of the Abl-related kinase, Arg. *J. Alzheimer's Dis. : JAD.* **19**, 721–733.
23. Maina, M.B., Al-Hilaly, Y.K., Burra, G., Rickard, J.E., Harrington, C.R., Wischik, C.M., (2021). Oxidative Stress Conditions Result in Trapping of PHF-Core Tau (297–391) Intermediates. *Cells.* **10**, 703.
24. Al-Hilaly, Y.K., Pollack, S.J., Vadukul, D.M., Citossi, F., Rickard, J.E., Simpson, M., (2017). Alzheimer's Disease-like Paired Helical Filament Assembly from Truncated Tau Protein Is Independent of Disulfide Crosslinking. *J. Mol. Biol.* **429**, 3650–3665.

25. Fitzpatrick, A.W.P., Falcon, B., He, S., Murzin, A.G., Murshudov, G., Garringer, H.J., (2017). Cryo-EM structures of tau filaments from Alzheimer's disease. *Nature* **547**, 185–190.
26. Al-Hilaly, Y.K., Foster, B.E., Biasetti, L., Lutter, L., Pollack, S.J., Rickard, J.E., (2019). Tau (297–391) forms filaments that structurally mimic the core of paired helical filaments in Alzheimer's disease brain. *FEBS Lett.*.
27. Lövestam, S., Koh, F.A., van Knippenberg, B., Kotecha, A., Murzin, A.G., Goedert, M., (2022). Assembly of recombinant tau into filaments identical to those of Alzheimer's disease and chronic traumatic encephalopathy. *Elife.* **11**
28. Maina, M.B., Burra, G., Al-Hilaly, Y.K., Mengham, K., Fennell, K., Serpell, L.C., (2020). Metal- and UV- Catalyzed Oxidation Results in Trapped Amyloid-β Intermediates Revealing that Self-Assembly Is Required for Aβ-Induced Cytotoxicity. *iScience.* **23**
29. Reynolds, M.R., Lukas, T.J., Berry, R.W., Binder, L.I., (2006). Peroxynitrite-Mediated τ Modifications Stabilize Preformed Filaments and Destabilize Microtubules through Distinct Mechanisms. *Biochemistry* **45**, 4314–4326.
30. Kondo, J., Honda, T., Mori, H., Hamada, Y., Miura, R., Ogawara, M., (1988). The carboxyl third of tau is tightly bound to paired helical filaments. *Neuron* **1**, 827–834.
31. Greenberg, S.G., Davies, P., (1990). A preparation of Alzheimer paired helical filaments that displays distinct tau proteins by polyacrylamide gel electrophoresis. *Proc. Natl. Acad. Sci. U S A.* **87**, 5827–5831.
32. Miao, J., Shi, R., Li, L., Chen, F., Zhou, Y., Tung, Y.C., (2019). Pathological Tau From Alzheimer's Brain Induces Site-Specific Hyperphosphorylation and SDS- and Reducing Agent-Resistant Aggregation of Tau in vivo. Frontiers in Aging. *Neuroscience* **11**
33. Gross, A.J., Sizer, I.W., (1959). The oxidation of tyramine, tyrosine, and related compounds by peroxidase. *J. Biol. Chem.* **234**, 1611–1614.
34. Galeazzi, L., Ronchi, P., Franceschi, C., Giunta, S., (1999). In vitro peroxidase oxidation induces stable dimers of β-amyloid (1–42) through dityrosine bridge formation. *Amyloid : Int. J. Exp. Clin. Investigat. : Off. J. Int. Soc. Amyl.* **6**, 7–13.
35. Souza, J.M., Giasson, B.I., Chen, Q., Lee, V.M., Ischiropoulos, H., (2000). Dityrosine cross-linking promotes formation of stable alpha -synuclein polymers. Implication of nitrative and oxidative stress in the pathogenesis of neurodegenerative synucleinopathies. *J. Biol. Chem.* **275**, 18344–18349.
36. Al-Hilaly, Y.K., Williams, T.L., Stewart-Parker, M., Ford, L., Skaria, E., Cole, M., (2013). A central role for dityrosine crosslinking of Amyloid-β in Alzheimer's disease. Acta Neuropathologica. *Communications.* **1**, 83.
37. Al-Hilaly, Y.K., Biasetti, L., Blakeman, B.J.F., Pollack, S.J., Zibaee, S., Abdul-Sada, A., (2016). The involvement of dityrosine crosslinking in α-synuclein assembly and deposition in Lewy Bodies in Parkinson's disease. *Sci. Rep.* **6**, 39171.
38. Lo Cascio, F., Garcia, S., Montalbano, M., Puangmalai, N., McAllen, S., Pace, A., (2020). Modulating disease-relevant tau oligomeric strains by small molecules. *J. Biol. Chem.* **295**, 14807–14825.
39. Lasagna-Reeves, C.A., Castillo-Carranza, D.L., Sengupta, U., Guerrero-Munoz, M.J., Kiritoshi, T., Neugebauer, V., (2012). Alzheimer brain-derived tau oligomers propagate pathology from endogenous tau. *Sci. Rep.* **2**, 700.
40. Atwood, C.S., Perry, G., Zeng, H., Kato, Y., Jones, W.D., Ling, K.Q., (2004). Copper mediates dityrosine cross-linking of Alzheimer's amyloid-beta. *Biochemistry* **43**, 560–568.
41. Pollack, S.J., Trigg, J., Khanom, T., Biasetti, L., Marshall, K.E., Al-Hilaly, Y.K., (2020). Paired Helical Filament-Forming Region of Tau (297–391) Influences Endogenous Tau Protein and Accumulates in Acidic Compartments in Human Neuronal Cells. *J. Mol. Biol.* **432**, 4891–4907.
42. Lutter, L., Al-Hilaly, Y.K., Serpell, C.J., Tuite, M.F., Wischik, C.M., Serpell, L.C., (2022). Structural Identification of Individual Helical Amyloid Filaments by Integration of Cryo-Electron Microscopy-Derived Maps in Comparative Morphometric Atomic Force Microscopy Image Analysis. *J. Mol. Biol.* **434**, 167466.
43. Labella, F., Keeley, F., Vivian, S., Thornhil, D., (1967). Evidence for Dityrosine in Elastin. *Biochem. Biophys. Res. Commun.* **26**, 748–1000.
44. Raven, D.J., Earland, C., Little, M., (1971). Occurrence of Dityrosine in Tussah Silk Fibroin and Keratin. *Biochim. Biophys. Acta.* **251**, 96.
45. Fujimoto, D., (1975). Occurrence of Dityrosine in Cuticlin, a Structural Protein from Ascaris Cuticle. *Comparative Biochem. Physiol. B-Biochem. Mol. Biol.* **51**, 205–207.
46. Waykole, P., Heidemann, E., (1976). Dityrosine in Collagen. *Connect. Tissue Res.* **4**, 219–222.
47. Skaff, O., Jolliffe, K.A., Hutton, C.A., (2005). Synthesis of the side chain cross-linked tyrosine oligomers dityrosine, trityrosine, and pulcherosine. *J. Org. Chem.* **70**, 7353–7363.
48. Souza, J.M., Giasson, B.I., Chen, Q.P., Lee, V.M.Y., Ischiropoulos, H., (2000). Dityrosine cross-linking promotes formation of stable alpha-synuclein polymers - Implication of nitrative and oxidative stress in the pathogenesis of neurodegenerative synucleinopathies. *J. Biol. Chem.* **275**, 18344–18349.
49. Van Der Vliet, A., Nguyen, M.N., Shigenaga, M.K., Eiserich, J.P., Marelich, G.P., Cross, C.E., (2000). Myeloperoxidase and protein oxidation in cystic fibrosis. *Am. J. Physiol. Lung Cell. Mol. Physiol.* **279**, L537–L546.
50. Leeuwenburgh, C., Hazen, S.L., Pennathur, S., Heinecke, J.W., (1996). Massive increase in protein-bound dityrosine in LDL isolated from human atherosclerotic aorta: Implications for the role of tyrosyl radical in atherogenesis. *Circulation* **94**, 2332.
51. Wells-Knecht, M.C., Huggins, T.G., Dyer, D.G., Thorpe, S. R., Baynes, J.W., (1993). Oxidized amino acids in lens protein with age. Measurement of o-tyrosine and dityrosine in the aging human lens. *J. Biol. Chem.* **268**, 12348–12352.
52. Bodaness, R.S., Zigler Jr., J.S., (1983). The rapid H2O2-mediated nonphotodynamic crosslinking of lens crystallins generated by the heme-undecapeptide from cytochrome C: potential implications for cataractogenesis in man. *Biochem. Biophys. Res. Commun.* **113**, 592–597.
53. Mayer, F., Pröpper, S., Ritz-Timme, S., (2014). Dityrosine, a protein product of oxidative stress, as a possible marker of acute myocardial infarctions. *Int. J. Legal Med.* **128**, 787–794.
54. Giulivi, C., Davies, K.J., (1993). Dityrosine and tyrosine oxidation products are endogenous markers for the selective proteolysis of oxidatively modified red blood cell

hemoglobin by (the 19 S) proteasome. *J. Biol. Chem.* **268**, 8752–8759.
55. Giulivi, C., Davies, K.J., (1994). Dityrosine: a marker for oxidatively modified proteins and selective proteolysis. *Methods Enzymol.* **233**, 363–371.
56. Kato, Y., Uchida, K., Kawakishi, S., (1994). Aggregation of collagen exposed to UVA in the presence of riboflavin: a plausible role of tyrosine modification. *Photochem. Photobiol.* **59**, 343–349.
57. Nunomura, A., Perry, G., Aliev, G., Hirai, K., Takeda, A., Balraj, E.K., (2001). Oxidative Damage Is the Earliest Event in Alzheimer Disease. *J. Neuropathol. Exp. Neurol.* **60**, 759–767.
58. Butterfield, D.A., Halliwell, B., (2019). Oxidative stress, dysfunctional glucose metabolism and Alzheimer disease. *Nat. Rev. Neurosci.* **20**, 148–160.
59. Lee, V.M., Balin, B.J., Otvos Jr., L., Trojanowski, J.Q., (1991). A68: a major subunit of paired helical filaments and derivatized forms of normal Tau. *Science* **251**, 675–678.
60. Zhang, W., Falcon, B., Murzin, A.G., Fan, J., Crowther, R. A., Goedert, M., et al., (2019). Heparin-induced tau filaments are polymorphic and differ from those in Alzheimer's and Pick's diseases. *eLife* **8**
61. Shi Y, Zhang W, Yang Y, Murzin A, Falcon B, Kotecha A, et al. Structure-based Classification of Tauopathies. bioRxiv. 2021:2021.05.28.446130.
62. Landino, L.M., Skreslet, T.E., Alston, J.A., (2004). Cysteine Oxidation of Tau and Microtubule-associated Protein-2 by Peroxynitrite: MODULATION OF MICROTUBULE ASSEMBLY KINETICS BY THE THIOREDOXIN REDUCTASE SYSTEM*. *J. Biol. Chem.* **279**, 35101–35105.
63. Saito, T., Chiku, T., Oka, M., Wada-Kakuda, S., Nobuhara, M., Oba, T., (2021). Disulfide bond formation in microtubule-associated tau protein promotes tau accumulation and toxicity in vivo. *Hum. Mol. Genet.* **30**, 1955–1967.
64. Weismiller, H.A., Holub, T.J., Krzesinski, B.J., Margittai, M., (2021). A thiol-based intramolecular redox switch in four-repeat tau controls fibril assembly and disassembly. *J. Biol. Chem.* **297**
65. Al-Hilaly, Y.K., Pollack, S.J., Rickard, J.E., Simpson, M., Raulin, A.-C., Baddeley, T., (2018). Cysteine-Independent Inhibition of Alzheimer's Disease-like Paired Helical Filament Assembly by Leuco-Methylthioninium (LMT). *J. Mol. Biol.* **430**, 4119–4131.